

Energy Distribution in Tin Halide Perovskite

Diego Di Girolamo,* Elena Blundo, Giulia Folpini, Corinna Ponti, Guixiang Li, Mahmoud H. Aldamasy, Zafar Iqbal, Jorge Pascual, Giuseppe Nasti, Meng Li, Roberto Avolio, Olga Russina, Alessandro Latini, Fahad Alharthi, Marco Felici, Annamaria Petrozza, Antonio Polimeni, and Antonio Abate*

The power conversion efficiency of the formamidinium tin iodide (FASI) solar cells constantly increases, with the current record power conversion efficiency approaching 15%. The literature reports a broad anomaly distribution of the photoluminescence (PL) peak position. The PL anomaly is particularly relevant to photovoltaic applications since it directly links the material's bandgap and subgap defects energy, which are crucial to extracting its full photovoltaic potential. Herein, the PL of FASI polycrystalline thin film and powder is studied. It is found that a distribution of PL peak positions in line with the distribution available in the literature systematically. The distribution in PL is linked to the octahedral tilting and Sn off-centering within the perovskite lattice, influenced by the procedure used to prepare the material. Our finding paves the way toward controlling the energy distribution of tin perovskite and thus preparing highly efficient tin halide perovskite solar cells.

1. Introduction

The replacement of toxic lead with less harmful tin could be a decisive step for the perovskite revolution of optoelectronics. Despite the increasing performances of tin perovskite solar cells, with power conversion efficiency (PCE) above 14%,^[1] the understanding of the fundamental properties and peculiarities of these semiconductors is still primordial.^[2–8] For instance, there is a certain degree of inconsistency in the literature when considering the bandgap of formamidinium tin iodide (FASI). In **Figure 1a**, we show the distribution of the bandgap (evaluated from various methods) and the photoluminescence (PL) maximum as found in articles published until 2020 for methylammonium lead iodide (MAPI) and FASI.^[9] For MAPI, considering more than 10⁴ values listed in 10 years, the bandgap is reproducibly reported

D. Di Girolamo, C. Ponti, G. Nasti, A. Abate
Department of Chemical
Materials and Production Engineering
University of Naples “Federico II”
Piazzale Vincenzo Tecchio 80, 80125 Naples, Italy
E-mail: diego.digirolamo@unina.it

E. Blundo, M. Felici, A. Polimeni
Department of Physics
University of Rome “La Sapienza”
Piazzale Aldo Moro 5, 00185 Rome, Italy

G. Folpini, A. Petrozza
Center for Nano Science and Technology @ PoliMi
Istituto Italiano di Tecnologia
20133 Milan, Italy

G. Li, M. H. Aldamasy, Z. Iqbal, J. Pascual, M. Li, A. Abate
Department of Novel Materials and Interfaces for Photovoltaic Solar Cells
Helmholtz-Zentrum Berlin für Materialien und Energie GmbH
Hahn-Meitner-Platz 1, 14109 Berlin, Germany
E-mail: antonio.abate@helmholtz-berlin.de

 The ORCID identification number(s) for the author(s) of this article can be found under <https://doi.org/10.1002/solr.202100825>.

© 2021 The Authors. Solar RRL published by Wiley-VCH GmbH. This is an open access article under the terms of the Creative Commons Attribution License, which permits use, distribution and reproduction in any medium, provided the original work is properly cited.

DOI: 10.1002/solr.202100825

M. Li
Key Lab for Special Functional Materials of Ministry of Education
National & Local Joint Engineering Research Center for High-efficiency
Display and Lighting Technology
School of Materials Science and Engineering
and Collaborative Innovation Center of Nano Functional Materials and
Applications
Henan University
Kaifeng 475004, China

R. Avolio
National Research Council of Italy
Institute for Polymers Composites and Biomaterials
Via Campi Flegrei 34, 80078 Pozzuoli (NA), Italy

O. Russina, A. Latini
Department of Chemistry
University of Rome “La Sapienza”
Piazzale Aldo Moro 5, 00185 Rome, Italy

F. Alharthi, A. Abate
Chemistry Department
College of Science
King Saud University
Riyadh 1145, Saudi Arabia

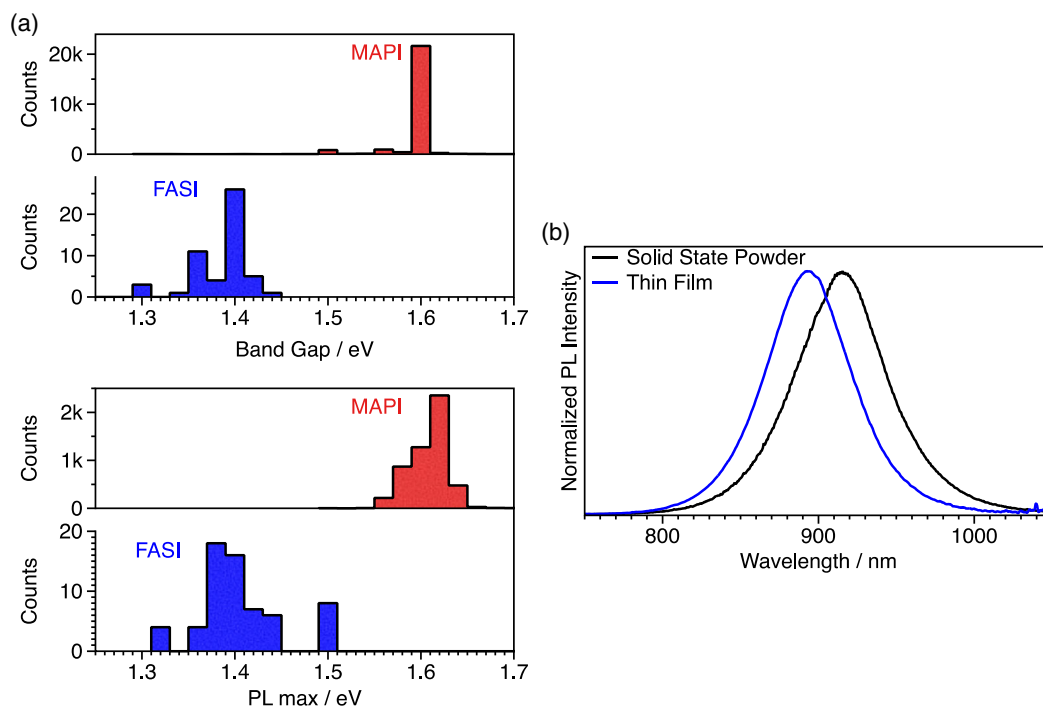


Figure 1. a) Histogram showing the distribution of bandgap (top) and PL maximum (bottom) for MAPI (in red) and FASI (in blue) as obtained from the literature published from 2009 to 2020. Note that there are 2–3 order of magnitude more data for MAPI than for FASI. b) Representative PL spectra at room temperature for FASI thin films (blue) and powder (black), showing a difference of about 30 nm in the wavelength maxima.

as 1.60 eV. A very narrow distribution of PL maximum around 770–774 nm (1.60–1.61 eV) has been observed. In the case of FASI, it isn't easy to estimate a single value from the bandgap and PL maxima. This finding is of particular interest, considering that the bandgap and the PL behaviors directly impact the photovoltaic efficiency.

The Burstein–Moss effect is generally invoked to rationalize shifts in the bandgap of tin halide perovskites.^[4] The spontaneous self p-doping of these materials, due to the low formation energy of the tin vacancy and the interstitial iodide defects^[6,10] or to the accidental oxidation of Sn,^[11,12] induces a photo-bleaching in the bandgap when probed through the light absorption due to the non-negligible population of holes at the valence band maximum.^[4] However, also the emission properties present a sizeable broadening. Emission from hot carriers might induce a blue-shift of the PL feature, but this mechanism has been observed only at high levels of illumination (>1–10 equivalent Sun).^[13] Discrepancies could also arise from self-absorption phenomena, as highlighted for large-sized single crystals of MAPI^[14] or trapping state emissions.^[14] Polymorphism and metastable phases are further reasonable hypotheses.^[15]

In this work, we study the variability in the PL properties of polycrystalline samples of FASI in the form of powder and thin films, aiming at highlighting different sources of PL energy variation. At variance with the previous literature, our results suggest that poor crystallinity and lattice distortion, leading to emission energy disorder, could be the decisive factor to explain the PL variation. Our results bring novel insight into the optoelectronic behavior of tin halide perovskites, suggesting that fine control

over the perovskite crystallization can be necessary to improve the material's quality.

2. Results and Discussion

Figure 1b shows that polycrystalline samples (i.e., powders and thin films) produced in a strictly anoxic environment leads to a broad PL peak at room temperature. In the case of the thin films, we have a PL peak at about 880–890 nm (i.e., 1.40 eV, see SI1 for a panoramic), while in the case of powder, the PL peak is found at around 910–915 nm (i.e., 1.36 eV). The result is reproducible in our conditions, with the synthesis performed in the same N₂ filled glove box where the PL is recorded. Moreover, similar PL (with substantial contribution above 900 nm) is found for different powder samples regardless of the synthetic procedure: 1) solid-state synthesis with mortar and pestle; 2) wet synthesis by shaking the precursors in tetrahydrofuran (THF); 3) wet synthesis by titrating with toluene a FASI solution in diethylformamide:N,N'-dimethylpropylene urea (DEF:DMPU) 6:1 solvent mixture, a chemical system from which we demonstrated working solar cells without the oxidizing dimethylsulfoxide (DMSO) solvent.^[16] In Figure SI2, Supporting Information, we show the PL of all such samples. Similarly, the PL obtained from the thin films is consistent regardless of the solvents and antisolvent used (Figure SI1, Supporting Information), and it is always blue-shifted than the PL of the powder. Self-absorption in the powder sample might account for part of the PL blue-shift. However, we measure in reflection mode while self-absorption is firmly impactful in transmission mode, where the emitted PL must

travel through the whole sample to be detected. In this condition, a 30-nm redshift has been observed for >2 mm thick MAPbBr₃ single crystals.^[17] In reflection mode, where the self-absorption depends on the charge generation profile and on the internal optical path the emitted light takes to escape from the front surface, Schötz reported a dual PL emission.^[18] At the same time, we observe a single light peak.

The blue shift of the PL of thin films could also be due to a larger self p-doping. However, this is not supported by the characterization of PL lifetimes in thin films and powders. Usually, tin perovskite films display sub-ns lifetimes due to an extensive background charge density, while adding SnF₂ or alloying 2D and 3D perovskites to reduce the self p-doping can result in longer lifetimes. First of all, a direct comparison of a lifetime in powders and thin films (Figure S13, Supporting Information) under comparable excitation conditions ($n \approx 10^{17} \text{ cm}^{-3}$) shows that the lifetimes of the decay are shorter in the case of the powders. This suggests a higher doping density in the powders compared with the films, pointing to a different origin of the PL blue shift.

In Figure S14, Supporting Information, we show that spatial non homogeneity accounts for a relevant share of the PL broadening of FASI powders, with micro-PL (μ -PL) spots showing differences in the emission wavelength. We remark that the μ -PL spot is in the range of $4 \mu\text{m}^2$, thus including several morphological grains (size in the 100-nm range, see Figure S15, Supporting Information). Our findings are in agreement with the results from Kontos et al.,^[19] who identified different PL emitting spots with PL maxima ranging from 892 to 918 nm in the same powder. Similar behavior was also observed in MASnI₃ and CsSnI₃.

The bandgap of metal halide perovskite results from the hybridization of halide and metal orbitals, here iodide 5p and tin 5s and 5p. The A-site cation (methylammonium, formamidinium, or caesium) impacts the bandgap by tuning the unit cell size and the octahedral distortion of the tin-iodide sublattice. The isotropic compression and expansion of the lattice (as obtained by variation in temperature within the stability range of the same crystal phase) is associated with a narrowing and widening bandgap, the opposite behavior of conventional semiconductors such as Si. The octahedral tilting, which is essential in the low temperature (and low symmetry) phases of metal halide perovskites, leads to a widening of the bandgap. At very low temperatures, the crystal structure of halide perovskites is generally orthorhombic and identified as the γ -phase.^[6,20,21] The lattice expands by heating these perovskites to room temperature and tends to assume a cubic (or pseudo-cubic) phase with no average octahedral tilting. A peculiarity of tin and lead halide perovskites is the possibility to undergo an unexpected symmetry decrease upon further warming, which is quite counterintuitive and was therefore named *emphansis*.^[22,23] The distortion does not affect the long-range order, and it is not associated with a phase transition. However, X-ray pair distribution functions reveal a structural disorder, interpreted as a mean off-centering of the B-site cation in the BX₃ octahedron. Emphasis is a relatively new phenomenon whose origin and mechanisms are still not entirely understood,^[24] but it has been observed for FASI at room temperature.^[7,25] The culprit is the lone pair on the M²⁺ B-site cation, more expressed in Sn²⁺ than in Pb²⁺, which plays a

stereochemical role. Indeed, in germanium halide perovskites (AGeX₃), with Ge²⁺ exacerbating the lone pair stereochemical activity, the emphasis is strongly pronounced in normal conditions and switched-off only at high pressures shown by pressure-dependent PL and structural characterizations.^[26] Crystal strain might also affect the degree of emphasis or the interplay between off-centering and octahedral tilting.^[27] A strain-dependent distribution of bandgaps has also been observed in high performances lead halide perovskite thin films.^[28] A similar mechanism is likely to occur with tin perovskites, where this effect is further amplified by the larger expression of the Sn²⁺ lone pair. Notably, a dual PL emission in FASI samples has been recently reported by Sekimoto and coworkers.^[29] They also attributed the phenomenon to the distribution of structural distortions by PL and NMR analysis.

The presence of a distribution of bandgaps within the photoactive layer of a solar cell might be problematic since the energetic disorder is generally linked to energy losses and recombination.^[30,31] Therefore, a deep understanding of the phenomenon is required to advance tin halide perovskites and bridge the gap with lead counterparts. Here, we provide further insights into the link between the PL distribution and crystallinity. We focused on mechanochemically synthesized powder to avoid any effect from solvents and anti-solvents, but we will discuss similarities and differences with thin films throughout the text.

In Figure 4, we show the temperature-dependent PL characterization of the mechanochemically synthesized FASI powder. By decreasing the temperature from 295 to 10 K, the PL red-shifts from 1.35 to 1.24 eV, while the intensity increases by a factor of 4.4. The redshift can be primarily explained by the lattice contraction, as depicted in Figure 2. In Figure 3b, we display the peak

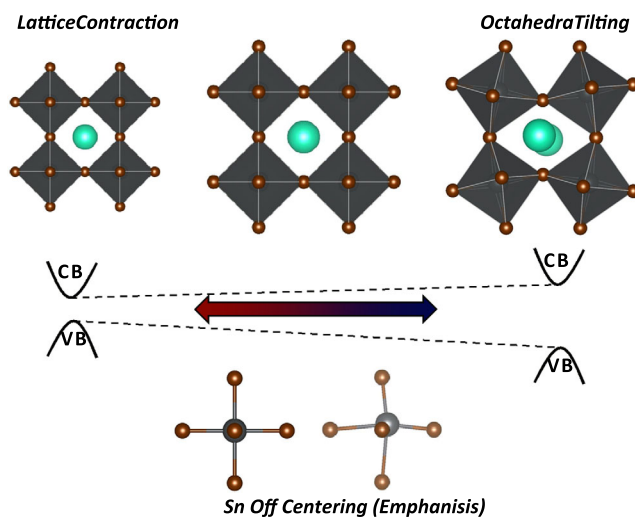


Figure 2. Perovskite lattice distortion (on top) and SnX₃ octahedron distortion (below) influence the bandgap. The more cubic the lattice and centered the Sn ion in the octahedron, the smaller the gap. The unit cell size, which could be influenced by temperature or strain, also affects the bandgap. The smaller the unit cell, the smaller the bandgap. The usual perovskite behavior is an increase in the symmetry of the lattice upon temperature increase (along with lattice expansion). However, at high temperatures, emphasis can emerge. It has been directly observed only in the cubic phase, notably at room temperature for FASI.

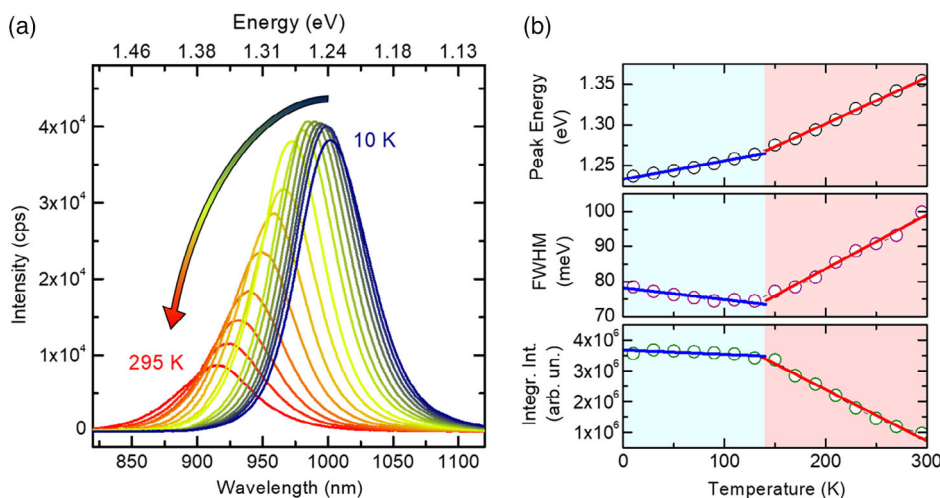


Figure 3. a) Macro-PL spectra of the powder as a function of temperature, from 295 to 10 K, in steps of ≈ 20 K. b) Peak energy, FWHM, and integrated intensity of the PL as a function of temperature. The red and blue lines are linear fits to the data in the temperature ranges from >150 to <150 K, respectively.

position, the full width at half maximum (FWHM) and the integrated intensity versus the temperature. We can notice an evident change in slope at around 150 K for all three observables, where the phase transition from tetragonal to orthorhombic phase occurs. Notably, the transition from cubic to tetragonal phase expected at 255 K is silent, as observed in single crystals and thin films by other groups.^[2] Thus, we observe a smooth variation of PL maxima and FWHM from 295 to 150 K, with a gradient of 0.6 and 0.15 meV K⁻¹, respectively. In the region below 100 K, the FWHM remains practically constant (the fit even suggests a slight increase). Kontos et al. observed a constant linewidth up to 250 K,^[19] while our results are more similar to the behavior of single crystals.^[2] The weak temperature dependence of the linewidth to temperature has been attributed to disorder or the presence of multiple emitting states.^[2] A sizeable difference between our results and those reported by Kahman on single crystals is found in the bandgap at 5–10 K: 1.24 eV in our case (and similar to thin films^[4]), larger than their 1.12 eV. Contrary to the FWHM behavior, the energy shift of the PL peak versus temperature features a noticeably different behavior in our case concerning the previous literature on thin films or single crystals. More specifically, Kahmann et al.^[2] found a redshift rate of ≈ 0.9 meV K⁻¹ in single crystals when decreasing T from RT to 50 K and a slightly lower rate at lower temperatures. In contrast, Kontos et al.^[19] observed a redshift rate of ≈ 0.3 meV K⁻¹ in thin films, in the range from 473 to 83 K. Curiously, our rate in the 300–150 K range falls in between (0.58 meV K⁻¹). However, for temperatures <150 K (and thus below the phase transition temperature), our redshift rate decreases to 0.22 meV K⁻¹. This lower rate can be tentatively attributed to larger structural distortions arising below the phase transition temperature. Since distortions such as the Sn²⁺ off-centering lead to a bandgap widening,^[19] this effect might compensate for the thermal shift and justify the rate decrease.

Along with a broad distribution, the PL of FASI displays a transient behavior under different conditions. By ageing the powder

in nitrogen for few weeks, it is possible to observe an evident narrowing of the PL peak and an overall redshift (Figure 4a). This also occurs if the powder is submerged in the solvent-antisolvent system, with similar kinetics (Supporting information, Figure S16, Supporting Information). Notably, the thermal annealing (100 °C for 1 h) is not essential here, as we could not observe a change in the peak shape (Supporting Information, Figure S17, Supporting Information). According to the model described in Figure 2, the redshift and narrowing of the PL peak points toward a relaxation of the material from a distorted material (octahedra tilting, emphasis) to a more ordered one.

We investigated the material's structure changes using X-ray diffraction (XRD) and solid-state NMR (ssNMR). Here, the samples need to go out of the glovebox for not more than a few days and, despite the excellent care, we cannot rule out completely the effects of air. Nonetheless, both characterization techniques indicate an increase in the crystallinity of the sample upon ageing in nitrogen. In the case of XRD (Figure 4b), the pristine sample (characterized within 24 h from the synthesis) is poorly crystalline, and the XRD peaks have a similar intensity to those attributed to SnI₂. This is not surprising since the mortar and pestle methods are efficient but rudimentary, and scarce control over the degree of completion of the synthesis is possible. Notably, after 30 days in the N₂ atmosphere, the perovskite crystallinity is strongly enhanced, while the SnI₂ peaks remain of similar magnitude. A possible reason for the redshift of PL could thus be the size of crystallites. From the Debye–Scherrer analysis we obtained a crystal size of 30 nm (which is a lower limit to the actual crystal size since the peak broadening is also instrumental and due to lattice strain). In lead halide perovskites, the bandgap for crystallites of size above 20 nm is considered as “size-independent,”^[32] and also recent theoretical calculation set the limit of quantum confinement well below the size of 30 nm.^[33] If tin perovskites behave similarly to lead ones in this respect it is reasonable to rule out the effect of (reduced) quantum confinement in the redshift of PL upon storage in nitrogen.

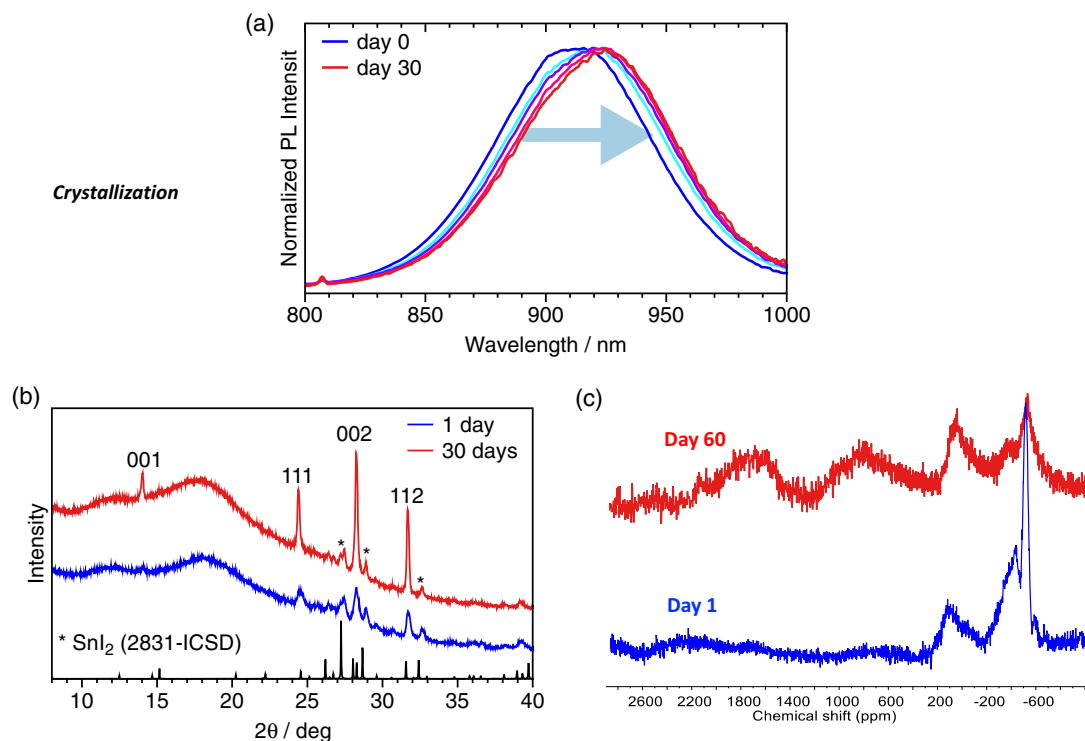


Figure 4. a) PL evolution over 20 days of FASI powder stored in an N₂-filled glovebox on a timescale of 20 days, showing an FWHM narrowing and an overall redshift. b) XRD of FASI powder measured the day after the synthesis and one month later. The latter sample showed more intense peaks. c) Solid-state NMR of FASI powder measured within the first 3 days from the synthesis and after about 2 months of storage in nitrogen. The intensity in the chemical shift range compatible with FASI is higher for the aged sample.

The trends obtained by ssNMR are consistent with those from XRD, even if the low signal intensity and broad line shapes do not allow further refining of the structural changes. Comparing the spectra of fresh and aged samples, it is possible to identify a signal about SnI₂ with a chemical shift of about -520 ppm, whose intensity is reduced after ageing. Moreover, in the aged sample, some new signal is observed in the range where the broad peak of FASI perovskite is expected,^[34] supporting a solid-state reaction of the powder components and a possible evolution toward perovskite (Figure 4c).

The PL redshift correlating with an increase in crystallinity of the perovskite sample is particularly interesting if we consider that slow improvements of device performances have been observed in tin perovskite solar cells^[35] and field-effect transistors.^[36] We could not observe a shift in the PL with time; however, slow dynamics has been reported for the crystallinity lead perovskite thin films.^[37,38]

When the perovskite is degraded, in contrast, the PL blue shifts. In Figure 5a,b, we report the PL evolution for FASI powder exposed to air. Figure 5d shows the normalized peaks and highlights a sequential blue shift within the first two hours of air exposure. Interestingly, by comparing the non-normalized spectra, we can observe a substantial increase in the PL intensity within the first few minutes of air exposure. After two hours of air exposure, the PL is blue-shifted by 30 nm yet with very similar intensity (notably, the same behavior can be also observed in thin films, see Figure S18, Supporting Information). Finally, the PL signal disappears after leaving the samples in the air overnight.

This behavior correlates with the XRD peak intensity of perovskite, showing a decrease within the first hour of exposure to air, as shown in Figure 5b. After waiting overnight, we observed peaks attributable to FA₂SnI₆, pointing to an extended degree of oxidation of FASI.

Nevertheless, the increase in the PL intensity of FASI powder upon short exposure to air is exciting (Figure 5c). The interaction of lead perovskites with oxygen (and moisture) has been thoroughly investigated for years (aiming at stabilizing and improving their performances), and a passivation mechanism from oxygen has been reported by many authors.^[39,40] In the case of tin perovskites, the rationalization of the interaction with oxygen has been limited to Sn oxidation and an increase in trap states. Thus, our observation might trigger further investigation. In addition, we also investigated the exposure of tin perovskite to iodine powder. Here, the oxidation was extremely fast, and we could not measure any PL beyond 1 h (Figure 5d). Also, in this case, during the oxidative degradation, the PL blue-shifts. This shows that it is essential to avoid the formation of iodine in the perovskite precursors solution^[41] or the accidental formation of iodine during PV operations.^[42,43]

3. Conclusions

This work reports new observations on the PL of FASI perovskites. We observe a broad distribution in the energy of the PL maximum in polycrystalline samples, which probably stems

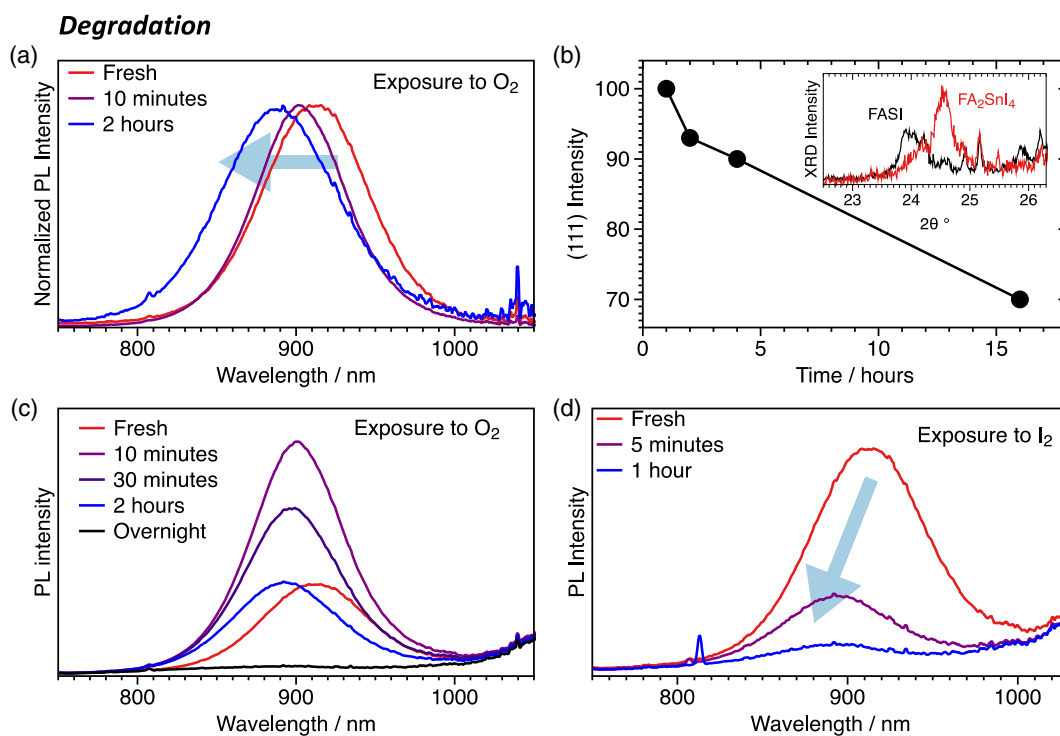


Figure 5. a) Normalized PL evolution of FASI powder exposed to air (the PL is measured in an N₂-filled glove box). A blue shift is observed. b) Relative variation of integrated intensity of (111) XRD peak of FASI during exposure to air, showing a decrease already in the first hour. After overnight exposure we observed the appearance of FA₂SnI₆ phase XRD peaks, as shown in the onset. The signal to noise ratio is low due to the necessity to follow the kinetics of the perovskite transformation, thus reducing the time to collect the diffractogram (see experimental). c) Same spectra as (a) not normalized, showing a non-monotonic variation in the PL intensity for short exposure to air. d) Normalized PL evolution of FASI powder exposed to I₂. A blue shift is observed, and we could no longer detect a strong PL signal after a few minutes.

from structural disorder amplified by the stereochemistry of the Sn²⁺ lone pair. Furthermore, we unveil the transient behavior of FASI PL: a redshift associated with a crystalline improvement is observed when the material is stored in N₂ for a few weeks, while oxidative stress from oxygen or iodine induces a fast blue-shift.

Our results provide new insights behind the structure–PL relationships in the FASI perovskite, suggesting that control over crystallinity should be targeted to increase devices’ performances and highlighting the importance of storage conditions on the properties of these materials.

4. Experimental Section

Chemicals and Materials: Formamidinium iodide was purchased from Dynameo. All the other chemicals were purchased from Sigma Aldrich and used as received.

Powder Synthesis: Solid-state synthesis was completed with pestle and mortar inside the glove box. A stoichiometric amount of FAI and SnI₂ are weighted inside the agate mortar for a total of 0.5–0.8 g of material and grinded until the powder is entirely black.

Wet synthesis was performed by titrating a DEF:DMPU 6:1 solution of FASI (1.5 M) with toluene. By adding a significant excess of toluene, FASI precipitation occurs. The supernatant was then removed, and the powder dried and annealed at 100 °C. Note that if toluene is not enough, the powder re-dissolves after precipitation. Another synthesis was carried out by shaking a vial containing FAI and SnI₂ powder in THF. THF does not dissolve FASI

but slightly dissolve FAI. Thus, mobile formamidinium and solvated iodide ions react with SnI₂. The black powder is formed almost immediately.

Thin Films Synthesis: Thin films have been deposited by spin coating with the anti-solvent method. For the film in Figure S11, Supporting Information, different solvents and antisolvent have been employed. In all cases, a 1.2 M FASI solution with SnI₂:FAI 1.1:1 stoichiometry was prepared and shaken overnight at room temperature. The film was spin-coated at 5000 rpm, and 100 μL of antisolvent was dispensed after the 30 s. Afterward, the films were annealed at 100 °C on the hot plate. The entire procedure was performed in an N₂-filled glovebox.

Characterization in Glove Box: The multimodal Arkeo machine has carried out the characterization in glovebox from Cicci Research Srl.

Photoluminescence test is performed with a commercial platform (ARKEO – Cicci Research): the substrate is illuminated with a diode-pumped solid-state (DPSS) Nd:YVO₄ + KTP Laser (Peak wavelength 532 ± 1 nm, Optical power 1 mW on a circular spot of 2 mm of diameter: 31 mW cm⁻²) at an inclination of 45°. The fluorescence on the same side of the substrate is focused on a bundle of fibers (10 mm in diameter) with an aspheric lens close to the substrate to maximize the PL. The bundle sends the signal to a CCD based spectrometer. Integration time and the number of averaging is maintained the same to better compare the results.

Macro-Photoluminescence Measurements: Macro-PL measurements versus temperature were performed in a He closed-cycle cryostat by Oxford instruments. The perovskite powder was deposited on a Cu substrate and encapsulated with thin glass. The sample was then glued by silver paint to the cold finger of the cryostat. The use of silver paint and the Cu substrate guarantee good thermal contact. The measurements were performed by exciting the sample with a 405-nm diode laser, focused on the sample by a lens in such a way to have a spot of ≈200 μm. The laser

power was measured before the lens. The emitted signal was collected by a CaF₂ lens and spectrally dispersed by a 200-cm focal length monochromator by Princeton Instruments equipped with a 150 groove mm⁻¹ grating blazed at 800 nm. The signal was then detected by a back-illuminated InGaAs array by Princeton Instruments. Since the InGaAs detector response decreases in the <1000 nm range, the spectra were corrected by considering the detector response. We also acquired measurements with a Si-CCD camera, updated them by considering the CCD response, and verified that there was good matching between the corrected spectra obtained with the two different detectors.

The measurements versus temperature were performed by cooling the sample down from room temperature (295 K) to 10 K, in steps of ≈20 K.

The room-temperature power study was performed by detecting the Si-CCD camera signal and normalizing it by the system response.

Micro-Photoluminescence Measurements: Micro-PL measurements were performed by exciting the sample with a 532-nm laser, focused on the sample by a 20× objective with NA = 0.4. The experiment was performed in a backscattering configuration, that is, the signal was collected by the same objective. The signal was then spectrally analyzed by the same monochromator and Si-CCD used for the macro-PL measurements.

Time-Resolved Photoluminescence: The measurements were performed analogously to micro-PL measurements, but the PL signal was excited by a pulsed supercontinuum laser. The laser's energy was tuned between 500 and 700 nm. Still, no sizeable variations were observed by changing the excitation wavelength after collecting the signal by the 20× objective, it was focused by a lens on an avalanche photodetector from MPD.

Time-Resolved PL on Thin Films: Tr-PL measurements were conducted using nitrogen-cooled Hamamatsu Time-Correlated Single Photon Counting (TCSPC) detector in a 1000 ns measurement window, corresponding to a temporal resolution of 700 ps (FWHM of the instrument response function). The decays were collected at the wavelength of the PL peak, 940 ± 5 nm. The sample was excited using a Chameleon oscillator (pulse duration 250 fs, 2 MHz repetition rate) with central wavelength 800 nm and average power varied between 1 uW and 500 mW. The beam was focused on the sample to a spot size of 40 μm radius. All measurements were performed on an encapsulated sample to avoid degradation upon air exposure.

ssNMR: The spectra were collected on a Bruker Avance II 400 spectrometer equipped with a 4-mm broadband Magic Angle Spinning (MAS) probe. Powder samples were packed in 4 mm zirconia rotors sealed with Vespel caps and spun at a rate of 12 or 13 kHz. A Direct Polarization (DP) scheme was applied, with a π/2 pulse width of 4 μs, a recycle delay of 40 s and averaging over 4096 scans.

X-Ray Diffraction: XRD was performed using a PANalytical X'Pert Pro MPD diffractometer (Cu Kα radiation), with patterns collected continuously (the time required to collect a single diffractogram is 1 h). The XRD analysis for the powder exposed to air was performed with a Bruker D8 Advance diffractometer equipped with a Mo Kα source as we did in our previous work.^[44] The XRD have been post corrected for the Kα₂, and the Bragg angles have been converted in the respective Cu Kα for an easier comparison with the previous data.

Scanning Electron Microscopy: The samples were analyzed using a field emission microscope Zeiss Auriga 405 with 1 nm nominal resolution (Oberkochen, Germany) equipped with a Bruker Quantax energy dispersive X-ray spectrometer (energy resolution: 123 eV K_α of Mn). Samples were observed under high vacuum (10⁻⁵–10⁻⁶ mbar).

Supporting Information

Supporting Information is available from the Wiley Online Library or from the author.

Acknowledgements

The Italian Ministry of Ecological Transition supported this work in the framework of the Operating Agreement with ENEA for Research on the

Electric System. The authors thank the Distinguished Scientist Fellowship Program (DSFP) at KSU for financial support. This work has received funding from the European Research Council (ERC) under the European Union's Horizon 2020 research and innovation programme (Grant agreement No. 804519). One of the authors (D.D.G.) thanks Francesco Mura for the SEM images.

Open access funding enabled and organized by Projekt DEAL.

Conflict of Interest

The authors declare no conflict of interest.

Data Availability Statement

Data available on request from the authors.

Keywords

lead-free perovskites, perovskite solar cells, photoluminescence

Received: October 5, 2021

Revised: November 19, 2021

Published online:

- [1] X. Jiang, H. Li, Q. Zhou, Q. Wei, M. Wei, L. Jiang, Z. Wang, Z. Peng, F. Wang, Z. Zang, K. Xu, Y. Hou, S. Teale, W. Zhou, R. Si, X. Gao, E. H. Sargent, Z. Ning, *J. Am. Chem. Soc.* **2021**, *143*, 10970.
- [2] S. Kahmann, O. Nazarenko, S. Shao, O. Hordichuk, M. Kepenekian, J. Even, M. V. Kovalenko, G. R. Blake, M. A. Loi, *ACS Energy Lett.* **2020**, *5*, 2512.
- [3] S. Kahmann, S. Shao, M. A. Loi, *Adv. Funct. Mater.* **2019**, *29*, 1902963.
- [4] R. L. Milot, M. T. Klug, C. L. Davies, Z. Wang, H. Kraus, H. J. Snaith, M. B. Johnston, L. M. Herz, *Adv. Mater.* **2018**, *30*, 1804506.
- [5] S. Gupta, D. Cahen, G. Hodes, *J. Phys. Chem. C* **2018**, *122*, 13926.
- [6] I. Chung, J. Song, J. Im, J. Androulakis, C. D. Malliakas, H. Li, A. J. Freeman, J. T. Kenney, M. G. Kanatzidis, *J. Am. Chem. Soc.* **2012**, *134*, 8579.
- [7] G. Laurita, D. H. Fabini, C. C. Stoumpos, M. G. Kanatzidis, R. Seshadri, *Chem. Sci.* **2017**, *8*, 5628.
- [8] I. Poli, G.-W. Kim, E. L. Wong, A. Treglia, G. Folpini, A. Petrozza, *ACS Energy Lett.* **2021**, *6*, 609.
- [9] T. J. Jacobsson, *Nat. Energy*, accepted.
- [10] D. Meggiolaro, D. Ricciarelli, A. A. Alasmari, F. A. S. Alasmay, F. De Angelis, *J. Phys. Chem. Lett.* **2020**, *11*, 3546.
- [11] M. I. Saidaminov, I. Spanopoulos, J. Abed, W. Ke, J. Wicks, M. G. Kanatzidis, E. H. Sargent, *ACS Energy Lett.* **2020**, *5*, 1153.
- [12] J. Pascual, G. Nasti, M. H. Aldamasy, J. A. Smith, M. Flatken, N. Phung, D. Di Girolamo, S.-H. Turren-Cruz, M. Li, A. Dallmann, R. Avolio, A. Abate, *Mater. Adv.* **2020**, *1*, 1066.
- [13] H.-H. Fang, S. Adjokatse, S. Shao, J. Even, M. A. Loi, *Nat. Commun.* **2018**, *9*, 243.
- [14] S. Narra, E. Jocar, O. Pearce, C.-Y. Lin, A. Fathi, E. W.-G. Diao, *J. Phys. Chem. Lett.* **2020**, *11*, 5699.
- [15] M. I. Dar, G. Jacopin, S. Meloni, A. Mattoni, N. Arora, A. Boziki, S. M. Zakeeruddin, U. Rothlisberger, M. Grätzel, *Sci. Adv.* **2016**, *2*, <https://doi.org/10.1126/sciadv.1601156>.
- [16] D. Di Girolamo, J. Pascual, M. H. Aldamasy, Z. Iqbal, G. Li, E. Radicchi, M. Li, S.-H. Turren-Cruz, G. Nasti, A. Dallmann, F. De Angelis, A. Abate, *ACS Energy Lett.* **2021**, *6*, 959.

- [17] B. Wenger, P. K. Nayak, X. Wen, S. V. Kesava, N. K. Noel, H. J. Snaith, *Nat. Commun.* **2017**, *8*, 590.
- [18] K. Schötz, A. M. Askar, W. Peng, D. Seeberger, T. P. Gujar, M. Thelakkat, A. Köhler, S. Huettner, O. M. Bakr, K. Shankar, F. Panzer, *J. Mater. Chem. C* **2020**, *8*, 2289.
- [19] A. G. Kontos, A. Kaltzoglou, M. K. Arfanis, K. M. McCall, C. C. Stoumpos, B. W. Wessels, P. Falaras, M. G. Kanatzidis, *J. Phys. Chem. C* **2018**, *122*, 26353.
- [20] M. Rodová, J. Brožek, *J. Therm. Anal.* **2003**, *71*, 667.
- [21] C. C. Stoumpos, C. D. Malliakas, M. G. Kanatzidis, *Inorg. Chem.* **2013**, *52*, 9019.
- [22] K. M. Ø. Jensen, E. S. Božin, C. D. Malliakas, M. B. Stone, M. D. Lumsden, M. G. Kanatzidis, S. M. Shapiro, S. J. L. Billinge, *Phys. Rev. B* **2012**, *86*, 085313.
- [23] E. Takeshi, S. J. L. Billinge, in *Pergamon Mater. Ser.* **2012**, pp. 371–405, <https://doi.org/10.1016/B978-0-08-097133-9.00009-5>.
- [24] K. Mukhuti, S. Sinha, S. Sinha, B. Bansal, *Appl. Phys. Lett.* **2021**, *118*, 162111.
- [25] E. C. Schueller, G. Laurita, D. H. Fabini, C. C. Stoumpos, M. G. Kanatzidis, R. Seshadri, *Inorg. Chem.* **2018**, *57*, 695.
- [26] X. Lü, C. Stoumpos, Q. Hu, X. Ma, D. Zhang, S. Guo, J. Hoffman, K. Bu, X. Guo, Y. Wang, C. Ji, H. Chen, H. Xu, Q. Jia, W. Yang, M. G. Kanatzidis, H.-K. Mao, *Natl. Sci. Rev.* **2021**, *8*, 288.
- [27] S. K. Radha, C. Bhandari, W. R. L. Lambrecht, *Phys. Rev. Mater.* **2018**, *2*, 063605.
- [28] T. W. Jones, A. Osherov, M. Alsari, M. Sponseller, B. C. Duck, Y.-K. Jung, C. Settens, F. Niroui, R. Brenes, C. V. Stan, Y. Li, M. Abdi-Jalebi, N. Tamura, J. E. Macdonald, M. Burghammer, R. H. Friend, V. Bulović, A. Walsh, G. J. Wilson, S. Lilliu, S. D. Stranks, *Energy Environ. Sci.* **2019**, *12*, 596.
- [29] T. Sekimoto, M. Suzuka, T. Yokoyama, Y. Miyamoto, R. Uchida, M. Hiraoka, K. Kawano, T. Sekiguchi, Y. Kaneko, *Cryst. Growth Des.* **2020**, *20*, 874.
- [30] M. H. Wolter, R. Carron, E. Avancini, B. Bissig, T. P. Weiss, S. Nishiwaki, T. Feurer, S. Buecheler, P. Jackson, W. Witte, S. Siebentritt, *Prog. Photovoltaics Res. Appl.* **2021**, 3449.
- [31] J. Wong, S. T. Omelchenko, H. A. Atwater, *ACS Energy Lett.* **2021**, *6*, 52.
- [32] Y.-H. Kim, C. Wolf, Y.-T. Kim, H. Cho, W. Kwon, S. Do, A. Sadhanala, C. G. Park, S.-W. Rhee, S. H. Im, R. H. Friend, T.-W. Lee, *ACS Nano* **2017**, *11*, 6586.
- [33] A. Ummadisingu, S. Meloni, A. Mattoni, W. Tress, M. Grätzel, *Angew. Chem., Int. Ed.* **2021**, *133*, 21538.
- [34] D. J. Kubicki, D. Prochowicz, E. Salager, A. Rakhmatullin, C. P. Grey, L. Emsley, S. D. Stranks, *J. Am. Chem. Soc.* **2020**, *142*, 7813.
- [35] M. Li, W. Zuo, Y. Yang, M. H. Aldamasy, Q. Wang, S. H. T. Cruz, S. Feng, M. Saliba, Z. Wang, A. Abate, *ACS Energy Lett.* **2020**, *5*, 1923.
- [36] S. Shao, W. Talsma, M. Pitaro, J. Dong, S. Kahmann, A. J. Rommens, G. Portale, M. A. Loi, *Adv. Funct. Mater.* **2021**, *31*, 2008478.
- [37] B. Roose, A. Ummadisingu, J. P. Correa-Baena, M. Saliba, A. Hagfeldt, M. Graetzel, U. Steiner, A. Abate, *Nano Energy* **2017**, *39*, 24.
- [38] C. Fei, H. Wang, *Org. Electron.* **2019**, *68*, 143.
- [39] D. Lu, Y. Zhang, M. Lai, A. Lee, C. Xie, J. Lin, T. Lei, Z. Lin, C. S. Kley, J. Huang, E. Rabani, P. Yang, *Nano Lett.* **2018**, *18*, 6967.
- [40] D. Meggiolaro, E. Mosconi, F. De Angelis, *ACS Energy Lett.* **2017**, *2*, 2794.
- [41] S. Chen, X. Xiao, H. Gu, J. Huang, *Sci. Adv.* **2021**, *7*, 1.
- [42] L. Lanzetta, T. Webb, N. Zibouche, X. Liang, D. Ding, G. Min, R. J. E. Westbrook, B. Gaggio, T. J. Macdonald, M. S. Islam, S. A. Haque, *Nat. Commun.* **2021**, *12*, 2853.
- [43] F. Fu, S. Pisoni, Q. Jeangros, J. Sastre-Pellicer, M. Kaweckı, A. Paracchino, T. Moser, J. Werner, C. Andres, L. Duchêne, P. Fiala, M. Rawlence, S. Nicolay, C. Ballif, A. N. Tiwari, S. Buecheler, *Energy Environ. Sci.* **2019**, *12*, 3074.
- [44] D. Di Girolamo, M. I. Dar, D. Dini, L. Gontrani, R. Caminiti, A. Mattoni, M. Graetzel, S. Meloni, *J. Mater. Chem. A* **2019**, *7*, 12292.